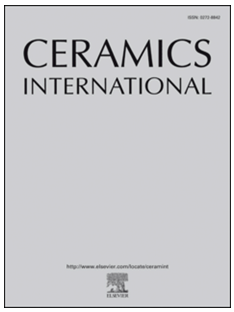

Influence of specimen size and microstructure on uniaxial compression of WC-Co micropillars

D.A. Sandoval, A. Rinaldi, A. Notargiacomo, O. Ther, E. Tarrés, J.J. Roa, L. Llanes

PII: S0272-8842(19)31211-8

DOI: https://doi.org/10.1016/j.ceramint.2019.05.102

Reference: CERI 21554

To appear in: *Ceramics International*

Received Date: 4 February 2019

Revised Date: 8 May 2019

Accepted Date: 10 May 2019

Please cite this article as: D.A. Sandoval, A. Rinaldi, A. Notargiacomo, O. Ther, E. Tarrés, J.J. Roa, L. Llanes, Influence of specimen size and microstructure on uniaxial compression of WC-Co micropillars, *Ceramics International* (2019), doi: https://doi.org/10.1016/j.ceramint.2019.05.102.

Influence of specimen size and microstructure on uniaxial compression of WC-Co micropillars

D.A. Sandoval[a,b,*], A. Rinaldi[c], A. Notargiacomo[d], O. Ther[e], E. Tarrés[e], J. J. Roa[a,b], L. Llanes[a,b]

[a] CIEFMA-Department of Materials Science and Metallurgy, EEBE-Campus Diagonal Besòs, Universitat Politècnica de Catalunya, Barcelona (Spain).

[b] Barcelona Research Center in Multiscale Science and Engineering, Campus Diagonal Besòs, Universitat Politècnica de Catalunya, Barcelona (Spain)

[c] Italian National Agency for New Technologies, Energy and Sustainable Economic Development (ENEA), Casaccia, Rome (Italy)

[d] Institute for Photonics and Nanotechnologies – CNR, Rome (Italy)

[e] Hyperion Materials & Technologies, Martorelles (Spain)

*Corresponding author e-mail: daniela.andreina.sandoval@upc.edu

Abstract

The current interest on the development of components on the micrometer size regime demands the evaluation of the mechanical behavior at such small length scales. Regarding cemented carbides, evaluation of mechanical properties at the micrometer scale is a relatively unexplored subject. In the present work we propose and validate a testing protocol based on uniaxial compression of micropillars milled by focused ion beam, to evaluate the elastic and plastic response of WC-Co alloys. In doing so, we studied three WC-Co alloys: fine, medium and coarse grained. First, we determined an appropriate Representative Elementary Volume (REV) to consider the tested sample as a bulk. Then, we performed uniaxial compression on the micropillars that met that REV. Based on the stiffness recorded for each micropillar, we found that the estimated elastic modulus for the fine and medium grained alloys is within the range expected for WC-Co alloys with a similar volume fraction of constitutive phases as those studied here. Finally, we stablished a correlation among stress-strain response, microstructure and yielding within constitutive phases by linking strain bursts taken place at different stress levels to plastic deformation/damage features observed in the micropillars after uniaxial compression.

Keywords

WC-Co composites, micropillar milling, uniaxial compression, micromechanics.

1. Introduction

WC-Co cemented carbides (usually referred to as hardmetals) are materials used widely in the tooling industry due to their elevated hardness, strength, elastic modulus, rigidity, and wear resistance. The outstanding mechanical and tribological response exhibited by them is a direct consequence of their microstructural assemblage: an interpenetrated network of two different phases (hard, brittle carbides and a soft, ductile metallic binder), with optimal interface properties [1–5]. In this regard, micromechanical models attempting to assess and predict performance of hardmetals have been developed regarding plastic deformation of the constrained metallic binder, microstructural aspects such as contiguity, shape and size of WC grains, and even anisotropy of the constitutive phases [6–8].

A common feature of above referred models is the consideration of specimens and components as a continuum, i.e. exhibiting bulk-like response because geometrical dimensions are large enough - with respect to microstructural length scale - such that surface-related influence may be neglected. However, the increasing interest on developing tool components within the decimeter to the micrometer size, yields cases where specimen dimensions are comparable to WC particle size. In this sense, it is well known that intrinsic properties of crystalline materials such as yield stress and strength are highly influenced by extrinsic factors such as surface/volume ratio [9–11]. Thus, known outstanding mechanical properties of cemented carbides might change with fabrication of smaller mechanical parts. Although the use of new advanced testing techniques has promoted research devoted to evaluate the mechanical response of cemented carbides at small length scales [12–15], the number of publications addressing size effects on these materials is

quite scarce. To the best knowledge of the authors, they reduce to three recent works with quite interesting findings: (1) increase of tensile strength from 2.5 to 6 GPa when varying the sample size from centimeter to micrometer regime [16]; (2) variation of elastic modulus and fracture strength with specimen size and Co area fraction within the sample [17]; and (3) transition of deformation/failure mechanisms, from those observed for WC crystals towards those discerned for bulk-like material, as diameter of compression tested micropillars increases from 1 to 4 microns, for a grade with carbide grain size about 1 micron [18].

In the present study we approach the size effect problem by considering the volume fraction of Co binder confined in a micropillar as key variable for rationalizing the mechanical response observed. Microstructural influence is investigated by conducting tests in three WC-Co grades exhibiting similar binder content but distinct carbide grain size: fine, medium and coarse. In that sense, we assumed that a sample of representative elementary volume (REV) of the bulk must have a volume fraction of Co binder near to that of the bulk. Afterwards, we conducted uniaxial compression tests on milled micropillars and by evaluation of stress-strain curves, we determined elastic modulus of the bulk, flow stress of the Co binder and reproducibility of the testing protocols implemented. Finally, we documented the mechanisms of plastic deformation observed after the compression tests. Results showed that size effect issue can be overcome by selecting an adequate REV. In this regard, uniaxial compression of micropillars could then be postulated as a powerful technique to optimize microstructural design of cemented carbides.

2. Materials and methods

2.1. Materials and samples

The studied materials are commercial grades of WC-Co alloys supplied by Hyperion Materials & Technologies. Three grades with similar binder content (around 10 wt.% of Co), and different WC mean grain size - classified as coarse (C), medium (M) and fine (F) - were selected. Field emission scanning electron microscopy (FESEM) images of the three materials studied are shown in **Figure 1**. Mean WC grain size was determined by means of linear intercept method using FESEM images. Carbide contiguity and binder's mean free path were estimated from empirical equations given in literature [3,19]. Microstructural and mechanical characteristics for the three WC-Co grades studied are shown in **Table I**. Sample surfaces were ground and diamond polished up to mirror-like surface finish, following a 6 μm to 1 μm polishing protocol with a two-step final stage using colloidal silica. As a result, surfaces with roughness levels lower than 10 nm were attained [18].

At least six micropillars of 2 μm in diameter ($d_{micropillar}$) were milled on each sample. Selection of micropillar diameter was done based on the results obtained by the authors in a previous study [18]. It yielded different $d_{WC}/d_{micropillar}$ ratios: 0.2, 0.6, and 1.2 for fine, medium and coarse grades, respectively. A two-stage milling process was done to decrease interaction of Ga^+ ions with the samples. The first step was done with a dual beam Zeiss Neon 40 FIB/FESEM, whereas the second one was done with a FEI-Helios Nanolab 600 dual-beam FIB. In both cases a Ga^+ ion source operated at 30 kV was used. An angle of incidence of ~36° and currents of 4nA and 500 pA for the

first and second stages respectively were used, as higher incidence angles and low currents decrease the dose of Ga^+ ions into the sample [20]. Aspect ratio (ratio between the micropillar length and its surface diameter) was kept between 2 and 4, in order to avoid sink-in upon compression and/or buckling of the micropillar. Taper angles were kept less than 5° to minimize errors in stress estimated from ideal strain-gradient free cylindrical micropillars. Before cross sectioning the micropillars, a protective Pt-based film was deposited in-situ in order to preserve the surfaces of the micropillars from damage from the Ga^+ ions. Final shape characteristics of micropillars are summarized in **Table II**. Representative FESEM images of one micropillar milled for each grade are shown in **Figure 2**.

2.2. Representative elementary volume (REV) analysis

To assure that the small-scale specimens were representative of the bulk materials, a study of the REV was done. In doing so, we based on the premise that a bulk-representative micropillar should exhibit similar volume fraction of constitutive phases to that measured in a material sample with large enough dimensions to avoid surface-related influence. To evaluate volume fraction of Co (V_{Co}), FESEM images of the complete surface of each micropillar were taken and volume fraction of Co was extracted by means of image analysis (IA) using free software FIJI ImageJ2. In order to correlate the Co volume fraction determined at the surface with the one measured at the entire volume of the micropillar, transversal sectioning of the micropillars was done in one micropillar of each WC-Co grade (**Figure 3**). Sectioning was done using Zeiss Neon 40 FIB/FESEM unit referred above. Before sectioning, a protective layer of platinum of around 1.5 μm in thickness was deposited on the entire surface of the micropillar to avoid interaction of the sample with Ga^+ ions.

Subsequent removing of material by milling at 100 pA, combined with imaging every 5 to 6 seconds, was done. Around 1000 images were obtained. Afterwards, surface fraction of Co in each image was estimated by IA following similar procedure as described before.

2.3. Uniaxial compression tests

Micropillars were uniaxially compressed in-situ using a nanoindenter INSEM Nanomechanics, placed inside a high-resolution field-emission-gun scanning electron microscope (FEG-SEM) LEO 35, Zeiss. The nanoindenter was equipped with a flat-diamond punch of 5 µm in nominal diameter. A schematic representation of the assembly and a view of the punch inside the SEM can be seen in **Figure 4**. Tests conducted were displacement-controlled, and load-displacement data was continuously recorded during the tests. Stress and strain were calculated with the area of the pillar at 1 µm of depth from the top surface, to avoid possible milling effects. This allows that variation of the stresses values, with respect to those calculated at the top of the micropillar, are the same for all grades. Total length of micropillars was used to determine strains. Nevertheless, after compression, definition of the effective gage length was unclear and variable. Plasticity phenomena in micropillars were usually evidenced in the middle/top part, a finding possibly linked to several reasons: first would be consideration that effective applied stress may decrease in the lower end of the micropillar, as related to slightly wider cross sections there; second cause could be the variable and continuously changing load transfer and distribution (between phases) from top to bottom, as soon as punch gets in contact with micropillar and irreversible phenomena starts to take place; final aspect to consider is the instantaneously wider (deformed) cross sections at the top of pillars and its influence on the effective stress there. Concomitant effect of all these issues is

quite difficult to quantify, and this directly applies to strain definition. For the present study we decided to follow same approach used by research community addressing micropillar compression testing [11,21,22], i.e. definition of strain using total pillar length. This would also be helpful for comparison purposes with other literature reports, as they have been implementing similar data analysis protocols.

Effective elastic deformation of both the indenter and the bulk material below the micropillar was extracted by an approach derived from Sneddon's equation [23,24]:

$$x_{Sneddon} = (1-\nu_i^2/E_i)*(F_{meas}/d_t) + (1-\nu_b^2/E_b)*(F_{meas}/d_b) \quad (1)$$

where $x_{Sneddon}$ is the displacement corrected by the Sneddon's approach, which is subtracted from the total displacement, F_{meas} is the measured force, d_t and d_b are the diameters of the micropillar at the top and bottom respectively, E_i and ν_i are elastic modulus and Poisson's ratio of the diamond tip (taken to be 1140 GPa and 0.07 respectively [25]), and E_b and ν_b correspond to elastic modulus and Poisson's ratio of each WC-Co grade (**Table I**). Calibration of the equipment was done with a Berkovich diamond-tip, on fused silica of elastic modulus equals to 72 GPa [25].

Maximum load and depth into the sample were imposed as 20 mN and 300 nm respectively, to standardize the tests. Such values were selected from tests performed previously in which elastic and plastic response was depicted before catastrophic failure took place [18]. The tests were

designed to stop when one of the two restrictions was achieved. After uniaxial compression, micropillars were sectioned and mechanisms of plastic deformation and damage on the surface and inside micropillars were inspected by means of FIB/FESEM.

3. Results and discussion

3.1. Evaluation of REV

Examples of binary images for the three cemented carbide grades studied are shown in **Figure 5**. White and black colors represent WC particles and Co binder respectively. At a glance, one can say that distribution of WC particles is more homogeneous in the fine-grained micropillar. On the other hand, distribution of both carbide and binder phases becomes more heterogeneous as microstructure gets coarser. This observation was true for all the micropillars investigated.

From the surface image analysis, we determined the volume fraction of Co binder in each micropillar ($V_{Co\text{-}p}$) and compared it with that measured in the volume of one sectioned micropillar for each grade. Since the differences in values were less than 5%, the volume fraction of Co binder measured at the surface of the micropillars may be considered as representative of the volume fraction of the binder across the whole micropillar. In **Table III** mean values of $V_{Co\text{-}p}$ are compared with mean values of volume fraction of Co binder in the bulk ($V_{Co\text{-}b}$). A clear tendency can be depicted: the larger WC mean grain size, the larger the differences of volume fraction of Co binder in the micropillar with respect to that existing in the bulk material. In this sense, we found that for the coarse grade the relative differences of volume fraction of Co binder between a micropillar and bulk material are higher than 40%. In addition, $V_{Co\text{-}p}$ is discerned to vary considerably from one to another micropillar. Two reasons may be recalled for explaining such deviation. First, micropillars were milled randomly in the surface of the samples. Second, WC mean grain size is

comparable to micropillar diameter (about 20% larger). Hence, micropillar itself for the coarse-grained material cannot longer be consider as a "large enough specimen"; and thus, it may not be taken as REV for this grade, i.e. micropillar volume is not representative of the bulk material. On the other hand, variation between mean values of $V_{Co\text{-}p}$ measured for fine and medium grades and those determined in the corresponding bulk materials are lower than 15%. Therefore, micropillars milled on fine and medium grades are concluded to satisfy the REV condition.

3.2. Stress-strain response and deformation mechanisms under uniaxial compression of micropillars

Following the REV approach discussed in section 3.1, we performed at least six in-situ uniaxial compression of micropillars on samples of fine and medium grade. **Figure 6** corresponds to stress-strain (σ-ε) curves plotted from recorded load-displacement (*P*-*h*) data. In both WC-Co grades, "strain hardening" is evidenced from the loading curve. However, a linear elastic load response is not evidenced, indicating an asymmetric response of the composite to applied stress, probably due to asymmetric thermal residual stresses (*trs*) relaxation during compression [26]. Reported values of elastic modulus – determined by impulse excitation vibration (IEV) method – for these grades are 577 ± 3 GPa and 582 ± 4 GPa for the medium and fine grades respectively [27]. Estimated elastic modulus (*E*) from the upper part of the unloading curve [25] was 430 ± 47 GPa for the medium grade and 625 ± 103 GPa for the fine grade, both values within the range of elastic modulus reported for Co (199 - 215 GPa) and WC (625 – 700 GPa) [28,29]. Although estimated values of elastic modulus of medium grade from this study differ from those experimentally measured by IEV, they are within the range of those expected for this two-phase material with a

WC volume fraction of around 0.8 [28]. These results corroborate, as expected, the tendency of a cemented carbide to exhibit higher elastic modulus with larger WC volume fraction.

Along the loading curve, strain bursts events ("pop-ins") can be identified. Such events occur at different strains for each test and can be associated with plastic deformation of both Co binder and WC, the latter being known for its ability to undergo considerable plastic deformation without the occurrence of brittle fracture [3]. In general, strain bursts take place at higher stress levels for the fine-grained material than for the coarse-grained one (**Figure 7**). Moreover, they are less numerous, for a given micropillar tested, in the former than in the later.

Several observations may be done regarding stress ranges (lower and upper bands) where pop-in events are found for each cemented carbide grade investigated (**Figure 8**). First, within the lower stress band (i.e. between 1 and 4 GPa) plasticity discerned must be directly related to deformation of the metallic binder. Here, the higher strength exhibited by the fine-grained micropillars, as compared to the one measured for the medium-grained ones, should be ascribed to the more pronounced constraining of the metallic binder in the former (smaller binder regions in **Figure 5**) than in the latter. It is in complete agreement with the Hall-Petch strengthening of the metallic phase first proposed and estimated by Sigl and coworkers [30,31], and recently validated by means of massive nanoindentation and statistical analysis by Roa *et al.* [32] in WC-Co alloys. Nevertheless, evidence of plastic events at stress values as low as 1.3 GPa in one medium-grained pillar points out the relevance of local heterogeneity of binder thickness in small-scale specimens. Although such value is still significantly higher than stress range where unconstrained Co binder

would be expected to deform plastically, i.e. between 0.4 and 0.8 GPa, depending on occurrence of fcc to hcp transformation and amount of W and C dissolved in the Co binder [33], it is also markedly lower than stress range where plasticity is expected to occur in bulk-like samples (i.e. above 2 GPa) with similar microstructure assemblage. Indeed, based on literature findings determined in either bulk [32,34] or micropillar [14] specimens, evidence of yielding associated with metallic binder within the range between 1 and 2 GPa requires either higher binder content or larger carbide grain size, i.e. effectively thicker binder layers.

Second, within the upper stress band (i.e. between 4 and 6 GPa), strain bursts identified should rather be linked to deformation taken place either at interface-related regions or within carbides themselves. Regarding the former, the use of high speed mechanical property mapping technique (involving 200,000 indents performed at maximum load of 4 mN within a 50 x 50 μm^2 area) have shown that hardness and also elastic modulus increase (with respect to that of constrained binder) when corresponding residual impressions are closer to WC/Co interfaces [35]. This phenomenon, possibly related to the elastic and plastic flow interaction of the metallic phase with the harder and stiffer WC particles, could then result in higher stress (i.e. above 4 GPa) for local yielding in such regions. Concerning carbides, although it is reported that they exhibit intrinsic yield stress values ranging between 6 and 7 GPa [12], plastic activity is clearly evidenced (to be shown in detail later) within some ceramic particles. In this regard, the intrinsic composite nature (i.e. independent of bulk-like or micropillar consideration) of cemented carbides should be recalled based on synergic interaction of deformation phenomena taking place within the constitutive phases. As it has been well-established in several studies involving modeling actions [5,36–38], regions neighboring geometry irregularities of particles as well as the wide range of thermal

residual stresses for WC (compressive in average but tensile in specific regions) due to particle shape and microstructure itself, may result in plasticity being developed at effective stresses lower than those measured in isolated WC single crystals.

Considering that elastic modulus values found in this study are within the ranges of what is expected for WC-Co alloys with similar microstructures to those studied here, and that plasticity events evidenced may be rationalized on the basis of: mechanical response reported for unconstrained and (variably) constrained binder, WC particles, and regions containing WC/WC and WC/Co interfaces; it may be stated that combination of an accurate selection of the REV and uniaxial compression of micropillars (following testing parameters proposed) allows reliable assessment of the mechanical properties of WC-Co cemented carbides. Nevertheless, it should be mentioned that there exist additional variables, not accounted in this study, which may affect the results reported here, e.g. local phase arrangement, orientation and distribution of WC particles, fcc to hcp initial ratio in Co binder, amount of W and C dissolved in the Co binder, and presence of grain growth inhibitors. Their effect should be addressed if an even deeper understanding of microstructure-mechanical response of these materials is attempted.

In accordance with strain bursts found in the indentation σ-ε curves, we observed plastic deformation phenomena by imaging the surface of micropillars by FESEM. Images of one representative micropillar of both grades are shown in **Figure 9**. As indicated is Section 2.3, detailed inspection of tested micropillars points out that irreversible deformation features are mainly discerned in the top and middle part of micropillars. Although it could affect strain

quantification, and possible reasons for such observation have already been commented above, emergence and evolution of individual phenomena are not expected to be affected by it. The first plasticity event we detected in both grades is the plastic flow of the Co binder located at the surface of the micropillar, i.e. within binder regions expected to be less constrained because of its surface nature. As expected, these events are less pronounced (at least less visible) in the fine-grained material than in the medium one, due to less presence of Co binder pools within micropillars, i.e. higher degree of constraint. Moreover, plastic flow of Co binder is often accompanied with the glide of WC particles in the fine-grained alloy, this being probably the reason for first pop-ins occurring at higher stresses than for the medium-grained one.

Further analysis of plastic deformation of Co binder can be done in the relatively large metallic pools found in the medium-grained grade. Deformation phenomena of Co binder comprise shape changes produced by dislocation movement and evolution of slip systems [33], fcc to hcp transformation [39] and twinning [40]. A staircase-like deformation is observed at some areas. Such structure can be attributed to the formation of piled-up groups of dislocations that travel on the same plane as a consequence of stair rod dislocation dipoles formed at the intersection of the leading partial of a dissociated dislocation with the fault [41,42].

Slip activity is also observed in WC particles in both WC-Co grades (**Figure 9**). In this case, plastic deformation is due to dislocations and stacking faults [43]. Early works on WC samples found that the predominant slip system is the $\{10\bar{1}0\}\langle 11\bar{2}3\rangle$ type with the splitting dislocation reaction $^1/_3[11\bar{2}3] \rightarrow {}^1/_6[11\bar{2}3] + {}^1/_6[11\bar{2}3]$ [44]. Most of the deformation observed is expected to be

linked to slip on the prismatic $\{10\bar{1}0\}$ planes, rather than on the basal or pyramidal ones, given that activation of other systems requires probably higher stresses than those reached in this study [34,45].

Besides irreversible deformation events, microcracking is also discerned in both tested materials. In the medium-grained grade microcracks occurred at WC/WC interfaces, and in less proportion at WC/Co ones. On the other hand, in the fine-grained alloy they are exclusively observed at WC/WC interfaces, probably due to the higher contiguity of this material, as compared to the coarser one. Low and high prominence of microcracks running along WC/Co or WC/WC interfaces respectively, points out high interface strength of the former and favorably nature to undergo damage at compressive loads of the latter. By cross-sectioning (see **Figure 10**), we observed that elongation of ductile enclaves and associated formation of microcavities within the binder takes place preferentially at the corners of the carbides (followed by crack propagation in some cases), i.e. points where stress and strain are intensified [31].

4. Conclusions

In the present work we proposed a protocol to evaluate mechanical properties and response of WC-Co alloys by means of uniaxial compression of micropillars. In doing so, we first evaluated the size effect in terms of sample size and microstructural features within samples. Then, we validated the proposed methodology by comparing the results obtained with those found in the literature for WC-Co at macro-scale. Based on the results, the following conclusion may be drawn:

1. An appropriate selection of a Representative Elementary Volume when performing uniaxial compression of micropillars on WC-Co overcomes the size effect issue. In this sense, the difference between the volume fraction for constitutive elements within the micropillars and that for the bulk should be less than 15% to avoid size effects.

2. By imposing maximum load and displacement of 20 mN and 300 nm, respectively, we reproduced the elastic response on each micropillar for each WC-Co grade tested, i.e. elastic modulus yielded values with low dispersion and within the range expected for WC-Co alloys with similar volume fraction of constitutive phases.

3. Uniaxial compression of micropillars allows to validate - by linking pop-in events found on stress-strain curves with deformation and damage features observed by means of FESEM

imaging - the effect of WC mean grain size on the constraining of the Co binder: higher in a fine-grained material than in a medium-grained one.

Acknowledgements

This investigation was partially supported by the Spanish Ministerio de Economía y Competitividad MINECO/FEDER through grant MAT2015-70780-C4-3-P, and by the industry-university collaborative program between Hyperion Materials & Technologies and UPC. D.A. Sandoval would like to acknowledge the support received by the COST Action CA15102 “Solutions for Critical Raw Materials under Extreme Conditions” as funding for a Short Term Scientific Mission at ENEA, and Dr. Trifon Trifonov at Barcelona Research Center in Multiscale Science and Engineering, for the support with FIB milling and sectioning of the micropillars.

References

[1] H.E. Exner, Physical and chemical nature of cemented carbides, Int. Mater. Rev. 4 (1979) 1149–73. doi:10.1179/imtr.1979.24.1.149.

[2] J. Gurland, New scientific approaches to development of tool materials, Int. Mater. Rev. 33 (1988) 151–166. doi:10.1179/imr.1988.33.1.151.

[3] B. Roebuck, E.A. Almond, Deformation and fracture processes and the physical metallurgy of WC-Co hardmetals, Int. Mater. Rev. 33 (1988) 90–112. doi:10.1179/095066088790324094.

[4] A. V. Shatov, S.S. Ponomarev, S.A. Firstov, R. Warren, The contiguity of carbide crystals of different shapes in cemented carbides, Int. J. Refract. Met. Hard Mater. 24 (2006) 61–74. doi:10.1016/j.ijrmhm.2005.03.003.

[5] E. Jiménez-Piqué, M. Turon-Vinas, H. Chen, T. Trifonov, J. Fair, E. Tarrés, L. Llanes, Focused ion beam tomography of WC-Co cemented carbides, Int. J. Refract. Met. Hard Mater. 67 (2017) 9–17. doi:10.1016/j.ijrmhm.2017.04.007.

[6] P.E. McHugh, P.J. Connolly, Micromechanical modelling of ductile crack growth in the binder phase of WC-Co, Comput. Mater. Sci. 27 (2003) 423–436. doi:10.1016/S0927-0256(03)00045-4.

[7] C.S. Kim, T.R. Massa, G.S. Rohrer, Modeling the relationship between microstructural features and the strength of WC-Co composites, Int. J. Refract. Met. Hard Mater. 24 (2006) 89–100. doi:10.1016/j.ijrmhm.2005.04.011.

[8] C.S. Kim, T.R. Massa, G.S. Rohrer, Modeling the influence of orientation texture on the strength of WC-Co composites, J. Am. Ceram. Soc. 90 (2007) 199–204. doi:10.1111/j.1551-2916.2006.01381.x.

[9] H. Zhang, B.E. Schuster, Q. Wei, K.T. Ramesh, The design of accurate micro-compression experiments, Scr. Mater. 54 (2006) 181–186. doi:10.1016/j.scriptamat.2005.06.043.

[10] J.L. Stewart, L. Jiang, J.J. Williams, N. Chawla, Prediction of bulk tensile behavior of dual phase stainless steels using constituent behavior from micropillar compression experiments, Mater. Sci. Eng. A. 534 (2012) 220–227. doi:10.1016/j.msea.2011.11.062.

[11] D.M. Dimiduk, M.D. Uchic, T.A. Parthasarathy, Size-affected single-slip behavior of pure nickel microcrystals, Acta Mater. 53 (2005) 4065–4077. doi:10.1016/j.actamat.2005.05.023.

[12] T. Csanádi, M. Bľanda, A. Duszová, N.Q. Chinh, P. Szommer, J. Dusza, Deformation characteristics of WC micropillars, J. Eur. Ceram. Soc. 34 (2014) 4099–4103. doi:10.1016/j.jeurceramsoc.2014.05.045.

[13] M. Trueba, A. Aramburu, N. Rodríguez, I. Iparraguirre, M.R. Elizalde, I. Ocaña, J.M. Sánchez, J.M. Martínez-Esnaola, “In-situ” mechanical characterisation of WC-Co hardmetals using microbeam testing, Int. J. Refract. Met. Hard Mater. 43 (2014) 236–240. doi:10.1016/j.ijrmhm.2013.12.005.

[14] J.M. Tarragó, J.J. Roa, E. Jiménez-Piqué, E. Keown, J. Fair, L. Llanes, Mechanical deformation of WC–Co composite micropillars under uniaxial compression, Int. J. Refract. Met. Hard Mater. 54 (2016) 70–74. doi:10.1016/j.ijrmhm.2015.07.015.

[15] D.A. Sandoval, J.J. Roa, O. Ther, E. Tarrés, L. Llanes, Micromechanical properties of WC-(W,Ti,Ta,Nb)C-Co composites, J. Alloys Compd. 777 (2019) 593–601. doi:10.1016/j.jallcom.2018.11.001.

[16] T. Klünsner, S. Wurster, P. Supancic, R. Ebner, M. Jenko, J. Glätzle, A. Püschel, R. Pippan, Effect of specimen size on the tensile strength of WC–Co hard metal, Acta Mater. 59 (2011) 4244–4252. doi:10.1016/j.actamat.2011.03.049.

[17] T. Namazu, T. Morikaku, H. Akamine, T. Fujii, Mechanical reliability of FIB-fabricated WC–Co cemented carbide nanowires evaluated by MEMS tensile testing, Eng. Fract. Mech. 150 (2015) 126–134. doi:10.1016/j.engfracmech.2015.07.007.

[18] D.A. Sandoval, A. Rinaldi, J.M. Tarragó, J.J. Roa, J. Fair, L. Llanes, Scale effect in mechanical characterization of WC-Co composites, Int. J. Refract. Met. Hard Mater. 72 (2018) 157–162. doi:10.1016/j.ijrmhm.2017.12.029.

[19] J.M. Tarragó, D. Coureaux, Y. Torres, F. Wu, I. Al-Dawery, L. Llanes, Implementation of an effective time-saving two-stage methodology for microstructural characterization of cemented carbides, Int. J. Refract. Met. Hard Mater. 55 (2016) 80–86. doi:10.1016/j.ijrmhm.2015.10.006.

[20] H.G. Jones, A.P. Day, D.C. Cox, Electron backscatter diffraction studies of focused ion beam induced phase transformation in cobalt, Mater. Charact. 120 (2016) 210–219. doi:10.1016/j.matchar.2016.09.004.

[21] M.D. Uchic, D.M. Dimiduk, A methodology to investigate size scale effects in crystalline plasticity using uniaxial compression testing, Mater. Sci. Eng. A. 400–401 (2005) 268–278. doi:10.1016/j.msea.2005.03.082.

[22] D.R.P. Singh, N. Chawla, G. Tang, Y.L. Shen, Micropillar compression of Al/SiC nanolaminates, Acta Mater. 58 (2010) 6628–6636. doi:10.1016/j.actamat.2010.08.025.

[23] B. Poon, D. Rittel, G. Ravichandran, An analysis of nanoindentation in linearly elastic solids, Int. J. Solids Struct. 45 (2008) 6018–6033. doi:10.1016/j.ijsolstr.2008.07.021.

[24] C.A. Volkert, E.T. Lilleodden, Size effects in the deformation of sub-micron Au columns, Philos. Mag. 86 (2006) 5567–5579. doi:10.1080/14786430600567739.

[25] W.C. Oliver, G.M. Pharr, An improved technique for determining hardness and elastic modulus using load and displacement sensing indentation experiments, J. Mater. Res. 7 (1992) 1564–1583. doi:10.1557/jmr.1992.1564.

[26] A. Krawitz, E. Drake, Residual stresses in cemented carbides - An overview, Int. J. Refract. Met. Hard Mater. 49 (2015) 27–35. doi:10.1016/j.ijrmhm.2014.07.018.

[27] J.M. Tarragó, S. Dorvlo, J. Esteve, L. Llanes, Influence of the microstructure on the thermal shock behavior of cemented carbides, Ceram. Int. 42 (2016) 12701–12708. doi:10.1016/j.ceramint.2016.05.024.

[28] H. Doi, Y. Fujiwara, K. Miyake, Y. Oosawa, A systematic investigation of elastic moduli of

WC-Co alloys, Metall. Mater. Trans. 1 (1970) 1417–1425. doi:10.1007/BF02900264.

[29] CES Edupack, Cambridge, UK, (2016).

[30] L.S. Sigl, H.F. Fischmeister, On the fracture toughness of cemented carbides, Acta Metall. 36 (1988) 887–897. doi:10.1016/0001-6160(88)90143-5.

[31] H.F. Fischmeister, S. Schmauder, L.S. Sigl, Finite element modelling of crack propagation in WC-Co hard metals, Mater. Sci. Eng. A. 105/106 (1988) 305–311. doi:10.1016/0025-5416(88)90711-2.

[32] J.J. Roa, E. Jiménez-Piqué, J.M. Tarragó, D.A. Sandoval, A. Mateo, J. Fair, L. Llanes, Hall-Petch strengthening of the constrained metallic binder in WC–Co cemented carbides: Experimental assessment by means of massive nanoindentation and statistical analysis, Mater. Sci. Eng. A. (2016). doi:10.1016/j.msea.2016.09.020.

[33] B. Roebuck, E.A. Almond, A.M. Cottenden, The influence of composition, phase transformation and varying the relative F.C.C. and H.C.P. phase contents on the properties of dilute Co-W-C alloys, Mater. Sci. Eng. 66 (1984) 179–194. doi:10.1016/0025-5416(84)90179-4.

[34] J.J. Roa, E. Jimenez-Pique, C. Verge, J.M. Tarragó, A. Mateo, J. Fair, L. Llanes, Intrinsic hardness of constitutive phases in WC-Co composites: nanoindentation testing, statistical analysis, WC crystal orientation effects and flow stress for the constrained metallic binder, J. Eur. Ceram. Soc. (2015) 3419–25. doi:10.1016/j.jeurceramsoc.2015.04.021.

[35] J.J. Roa, P. Sudharshan Phani, W.C. Oliver, L. Llanes, Mapping of mechanical properties at microstructural length scale in WC-Co cemented carbides: Assessment of hardness and elastic modulus by means of high speed massive nanoindentation and statistical analysis, Int. J. Refract. Met. Hard Mater. 75 (2018) 211–217. doi:10.1016/J.IJRMHM.2018.04.019.

[36] V. Livescu, B. Clausen, J.W. Paggett, A.D. Krawitz, E.F. Drake, M.A.M. Bourke, Measurement and modeling of room temperature co-deformation in WC-10wt.% Co, Mater. Sci. Eng. A. 399 (2005) 134–140. doi:10.1016/j.msea.2005.02.024.

[37] A.D. Krawitz, A.M. Venter, E.F. Drake, S.B. Luyckx, B. Clausen, Phase response of WC-Ni to cyclic compressive loading and its relation to toughness, Int. J. Refract. Met. Hard Mater. 27 (2009) 313–316. doi:10.1016/j.ijrmhm.2008.11.010.

[38] W. Kayser, A. Bezold, C. Broeckmann, Simulation of residual stresses in cemented carbides, Int. J. Refract. Met. Hard Mater. 63 (2017) 55–62. doi:10.1016/J.IJRMHM.2016.04.001.

[39] A.H. Graham, J.L. Youngblood, Work strengthening by a deformation-induced phase transformation in “MP alloys,” Metall. Mater. Trans. B. 1 (1970) 423–430. doi:10.1007/BF02811551.

[40] L. Remy, Kinetics of f.c.c. deformation twinning and its relationship to stress-strain behaviour, Acta Metall. 26 (1978) 443–451. doi:10.1016/0001-6160(78)90170-0.

[41] K. Rajan, J.B. Vander Sande, Room temperature strengthening mechanisms in a Co-Cr-Mo-C alloy, J. Mater. Sci. 17 (1982) 769–778. doi:10.1007/BF00540374.

[42] K. Rajan, Stacking fault strengthening in low stacking fault energy alloys, Scr. Metall. 17 (1983) 101–104. doi:10.1016/0036-9748(83)90079-0.

[43] E.A. Almond, B. Roebuck, The origin of WC substructure and the effect of processing on the microstructure of WC-Co hardmetals, in: 10th Plansee Semin. Vol. 1, Metallwerk Plansee Austria, 1981.

[44] M.K. Hibbs, R. Sinclair, Room-temperature deformation mechanisms and the defect structure of tungsten carbide, Acta Metall. 29 (1981) 1645–1654. doi:10.1016/0001-6160(81)90047-X.

[45] X. Liu, J. Zhang, C. Hou, H. Wang, X. Song, Z. Nie, Mechanisms of WC plastic deformation in cemented carbide, Mater. Des. 150 (2018) 154–164. doi:10.1016/j.matdes.2018.04.025.

List of figures

Figure 1. FESEM secondary electron micrographs of the microstructure of the materials investigated: a) fine, b) medium and c) coarse WC-Co grades.

Figure 2. FESEM images of micropillars of around 2 μm in diameter milled by means of FIB in a) fine, b) medium and c) coarse WC-Co grades.

Figure 3. Representation of FIB sectioning of one micropillar. The external coating of Pt allowed to avoid interaction of Ga+ with the micropillar to preserve its shape and size.

Figure 4. a) Scheme of the nanoindenter-sample assembly inside the SEM. b) In-situ view of the diamond tip placed on top of one micropillar.

Figure 5. Binary images of the surface of one micropillar of each WC-Co grade: a) fine, b) medium, and c) coarse. After treating the original images with ImageJ2 free software, the volume fraction of the Co binder phase (black phase inside the micropillar) was measured with the same software.

Figure 6. Stress-Strain (σ-ε) curves for a) fine, and b) medium WC-Co grades studied. Stresses were calculated at 1μm in depth from the top of the micropillars to avoid any effect from particle arrangement near the tip-micropillar engage area.

Figure 7. Plot representing strain bursts (pop-in) events and their order of occurrence (from 1st to 5th) in micropillars of a) fine and b) medium WC-Co grades.

Figure 8. Plastic/deformation phenomena scenario exhibited by WC-Co micropillars under uniaxial compression.

Figure 9. SEM images of the surface of one micropillar of 2μm in diameter after uniaxial compression in a) fine and b) medium WC-Co grades. Identified failure mechanisms are marked with arrows and numbered as follows: (1) plastic flow of the binder; (2) cracks at the WC/WC interfaces; (3) Glide of WC particles at WC/WC interfaces; (4) plastic deformation of WC particles (slip bands); and (5) plastic deformation of binder.

Figure 10. FIB-Cross section of near the centre of the micropillar of a) fine and b) medium grades of WC-Co. Failure mechanisms identified with arrows correspond to the following: (1) plastic flow of the binder; (2) cracks at the WC/WC interfaces; (3) Glide of WC particles at WC/WC interfaces; (6) cracks at WC/Co interfaces running close to WC particles.

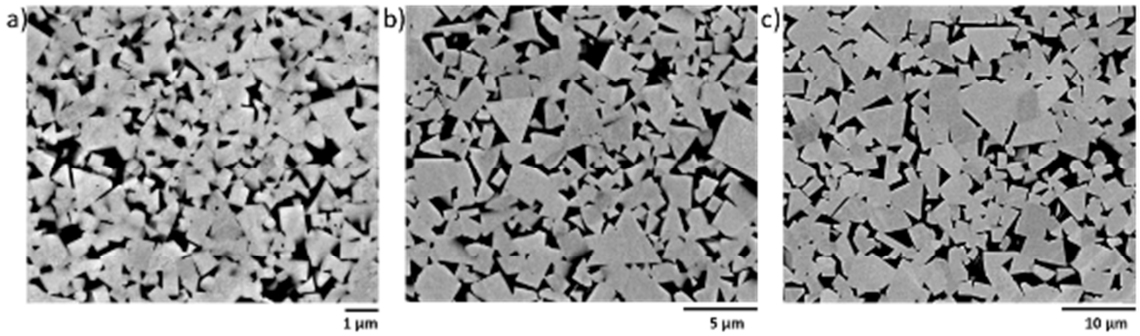

Figure 1. FESEM secondary electron micrographs of the microstructure of the materials investigated: a) fine, b) medium and c) coarse WC-Co grades.

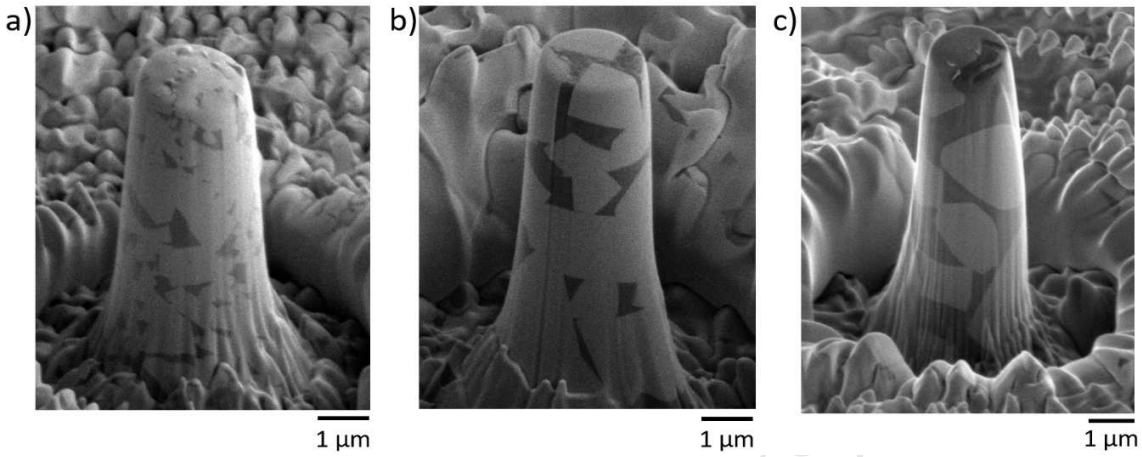

Figure 2. FESEM images of micropillars of around 2 µm in diameter milled by means of FIB in a) fine, b) medium and c) coarse WC-Co grades.

Figure 3. Representation of FIB sectioning of one micropillar. The external coating of Pt allowed to avoid interaction of Ga^+ with the micropillar to preserve its shape and size.

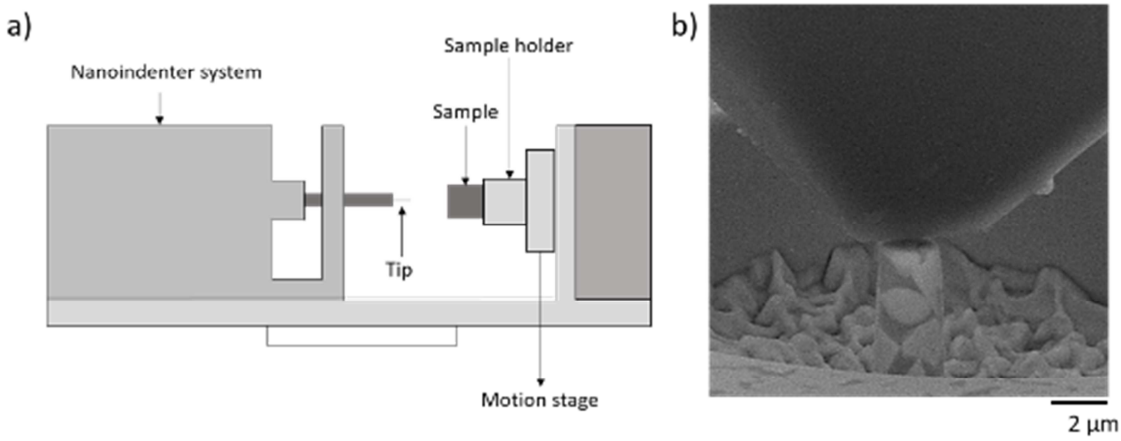

Figure 4. a) Scheme of the nanoindenter-sample assembly inside the SEM. b) In-situ view of the diamond tip placed on top of one micropillar.

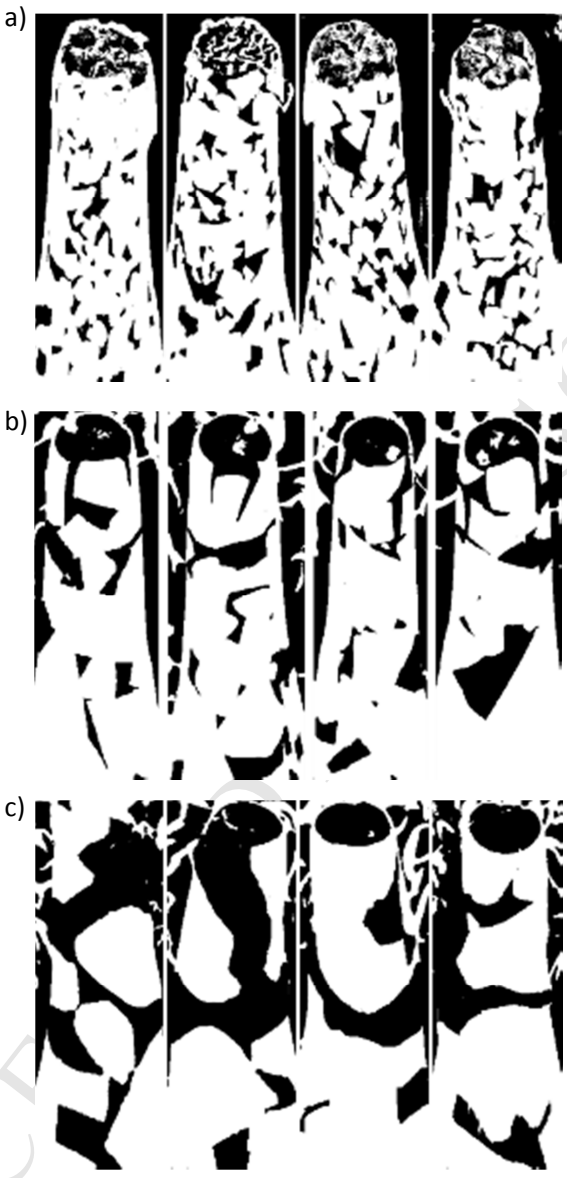

Figure 5. Binary images of the surface of one micropillar of each WC-Co grade: a) fine, b) medium, and c) coarse. After treating the original images with ImageJ2 free software, the volume fraction of the Co binder phase (black phase inside the micropillar) was measured with the same software.

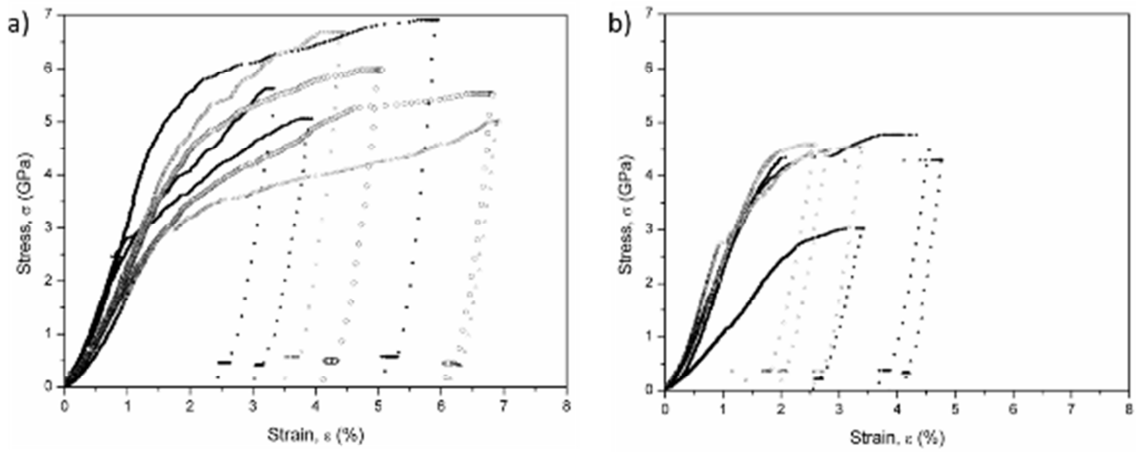

Figure 6. Stress-Strain (σ-ε) curves for a) fine, and b) medium WC-Co grades studied. Stresses were calculated at 1μm in depth from the top of the micropillars to avoid any effect from particle arrangement near the tip-micropillar engage area.

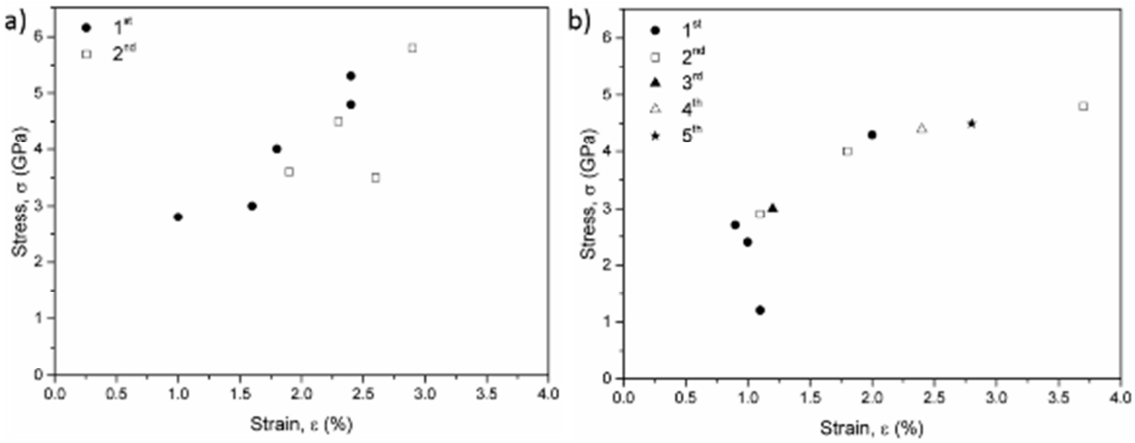

Figure 7. Plot representing strain bursts (pop-in) events and their order of occurrence (from 1st to 5th) in micropillars of a) fine and b) medium WC-Co grades.

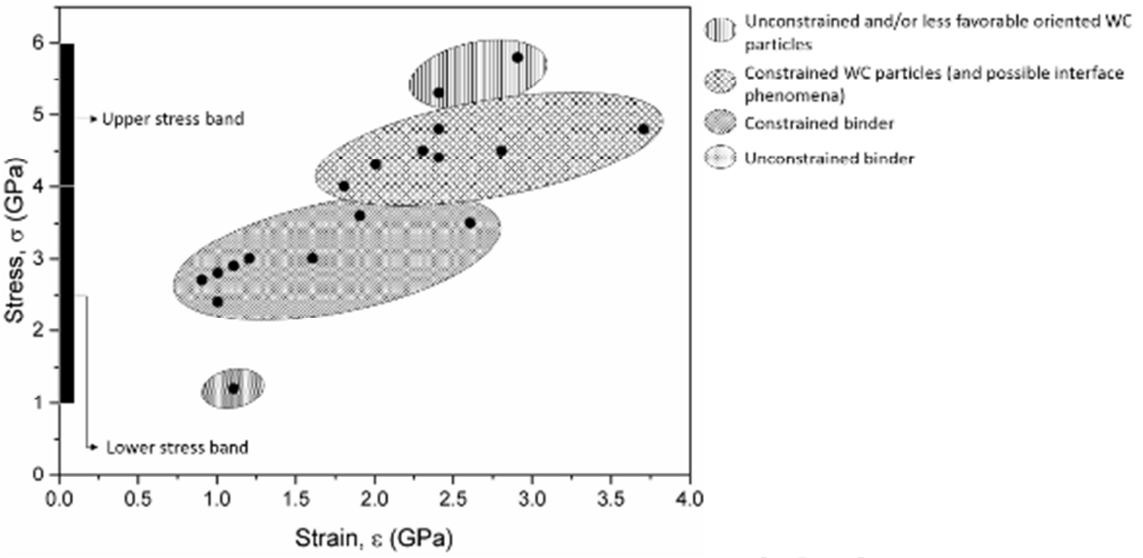

Figure 8. Plastic/deformation phenomena scenario exhibited by WC-Co micropillars under uniaxial compression.

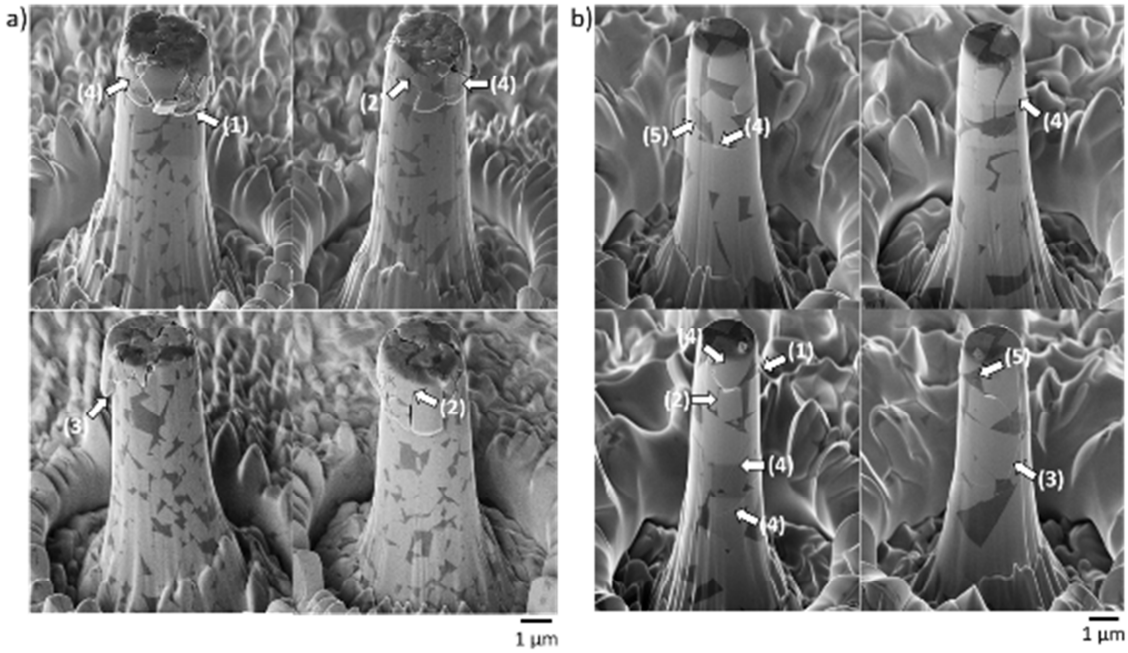

Figure 9. SEM images of the surface of one micropillar of 2µm in diameter after uniaxial compression in a) fine and b) medium WC-Co grades. Identified failure mechanisms are marked with arrows and numbered as follows: (1) plastic flow of the binder; (2) cracks at the WC/WC interfaces; (3) Glide of WC particles at WC/WC interfaces; (4) plastic deformation of WC particles (slip bands); and (5) plastic deformation of binder.

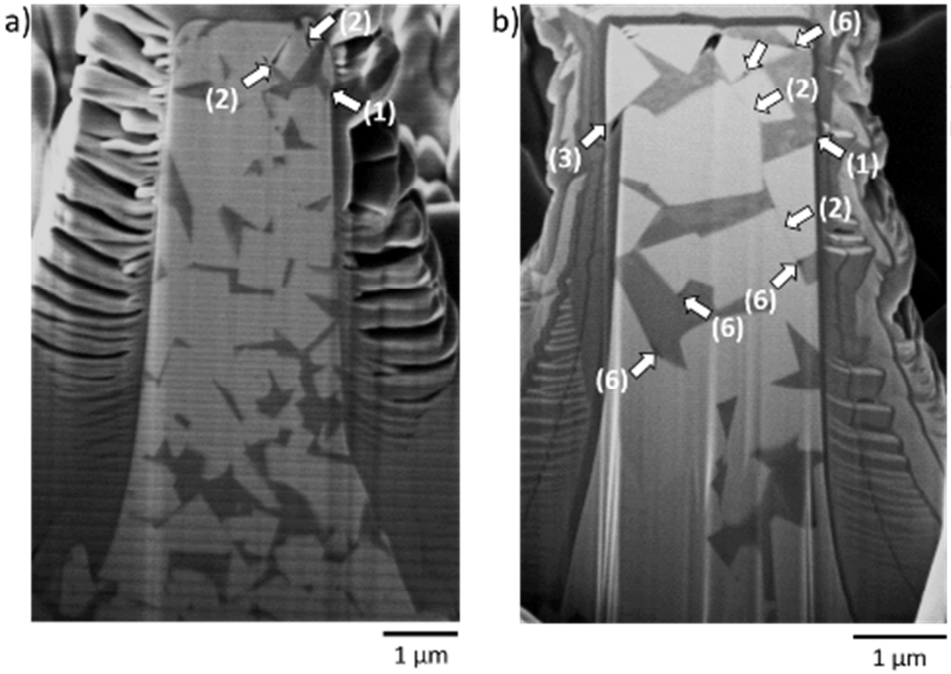

Figure 10. FIB-Cross section of near the centre of the micropillar of a) fine and b) medium grades of WC-Co. Failure mechanisms identified with arrows correspond to the following: (1) plastic flow of the binder; (2) cracks at the WC/WC interfaces; (3) Glide of WC particles at WC/WC interfaces; (6) cracks at WC/Co interfaces running close to WC particles.

List of tables

Table I. Microstructural characteristics: amount of Co binder in wt.% (Co *wt.%*), mean carbides grain size (*dWC*), binder mean free path (*λCo*) and contiguity of the carbide phase (*CWC*); and mechanical properties: elastic modulus (E), Poisson's ratio (*v*), Vickers Hardness (*HV30*), fracture toughness (KIc)for the three cemented carbide grades studied [27].

Table II. Shape and size parameters for the micropillars milled in each WC-Co grade studied: diameter at the top of the micropillar (*dt*), length/diameter ratio (*l/dt*), and tapper angle (*α*).

Table III. Mean volume fraction of Co binder in micropillars (*VCo-p*) measured by image analysis of the surface of each micropillar compared to volume fraction of Co binder in bulk material (*VCo-b*).

Table I. Microstructural characteristics: amount of Co binder in wt.% (Co *wt.%*), mean carbides grain size (d_{WC}), binder mean free path (λ_{Co}) and contiguity of the carbide phase (C_{WC}); and mechanical properties: elastic modulus (E), Poisson's ratio (ν), Vickers Hardness (HV_{30}), fracture toughness (K_{Ic})for the three cemented carbide grades studied [27].

Grade	**Co *wt.%***	**d_{WC} (μm)**	**λ_{Co} (μm)**	**C_{WC}**	**E (GPa)**	**ν**	**HV_{30} (GPa)**	**K_{Ic} (MPa√m)**
Fine (F)	10	0.4 ± 0.2	0.5 ± 0.1	0.2 ± 0.1	582 ± 4	0.24	15.7 ± 0.6	10.4 ± 0.3
Medium (M)	11	1.1 ± 0.7	0.4 ± 0.3	0.4 ± 0.1	577 ± 3	0.24	12.8 ± 0.2	13.9 ± 0.3
Coarse (C)	10	2.3 ± 1.4	0.7 ± 0.5	0.3 ± 0.1	595 ± 5	0.24	11.4 ± 0.2	15.8 ± 0.3

Table II. Shape and size parameters for the micropillars milled in each WC-Co grade studied: diameter at the top of the micropillar (d_t), length/diameter ratio (l/d_t), and tapper angle (α).

Grade	d_t (µm)	l/d_t	α (°)
Fine (F)	2.1 ± 0.0	3.3 ± 0.1	3.4 ± 0.5
Medium (M)	2.0 ± 0.1	3.7 ± 0.1	3.2 ± 0.5
Coarse (C)	1.9 ± 0.1	3.9 ± 0.2	3.1 ± 0.5

Table III. Mean volume fraction of Co binder in micropillars ($V_{Co\text{-}p}$) measured by image analysis of the surface of each micropillar compared to volume fraction of Co binder in bulk material ($V_{Co\text{-}b}$).

Grade	$V_{Co\text{-}p}$ (%)	$V_{Co\text{-}b}$ (%)
Fine (F)	16 ± 3	16
Medium (M)	20 ± 5	17
Coarse (C)	24 ± 10	16